# SUPPLEMENTARY MATERIALS

## Dual-frequency impedance assays for intracellular components in microalgal cells

Tao Tang[1], Xun Liu[1], Yapeng Yuan[2], Ryota Kiya[1], Yigang Shen[2], Tianlong Zhang[1,3], Kengo Suzuki[4], Yo Tanaka[2], Ming Li[3], Yoichiroh Hosokawa[1] and Yaxiaer Yalikun[1,2*]

1. Division of Materials Science, Nara Institute of Science and Technology, 8916-5 Takayama-cho, Ikoma, Nara 630-0192, Japan.
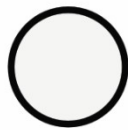
2. Center for Biosystems Dynamics Research (BDR), RIKEN, 1-3 Yamadaoka, Suita, Osaka, 565-0871, Japan.

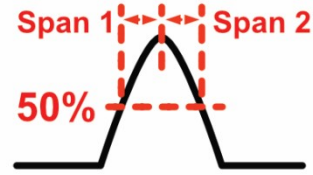3. School of Engineering, Macquarie University, Sydney, 2109, Australia.

4. Euglena Co. Ltd., Tokyo 108-0014, Japan;

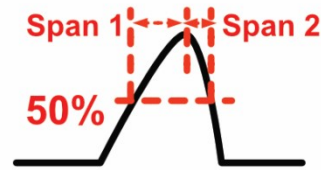# 1.     Tilt index

**Symmetric shape**     **Impedance pulse**

Span 1 ←→ ←→ Span 2

50%

Tilt index = 0

Tilt index = 0

**Asymmetric shape**     **Impedance pulse**

Span 1 ←--→← Span 2

50%

Tilt index > 0

Tilt index < 0

Fig. S1 Numerical simulation of tiling impedance pulse analysis for *E. gracilis* cells having different morphologies.

Similar to the simulation results (see Fig. S1), the impedance pulse for 10 μm beads is not tilted, but the impedance pulse triggered by *E. gracilis* is tilted due to the asymmetric shape of *E. gracilis* (see Fig.1D). To better characterize this phenomenon, we provided a new metric – tilt index, defined as:

$$tilt\ index = \frac{span\ 1}{span\ 2} - 1$$

(1)

The critical line is 50% peak value, and the tilt index is calculated as the ratio of the time spans on either side of the pulse peak and then subtracted by one, so that the metric is independent on the time-related parameters (i.e., flow rate) and the number fluctuates around zero. Theoretically, symmetric beads (e.g., Fig. S1) have a tilt index of almost zero, and the tilt index of most *E. gracilis cells* is greater than zero. More specifically, the tilt index tends to be zero for symmetric objects, while the tilt index tends to be greater than zero for non-symmetric objects. The degree of asymmetry of an object can also be quantified as a specific value by the tilt index. Notably, the sign of tilt index only indicates the orientation of the samples in the detection area.

# 2.    FPGA-based Detection circuit



Fig. S2: Experimental setup. (A) Schematic diagram of the detection method, including the specific hardware devices. (B) FPGA-based Lock-in amplifier and involved digital signal processing methods. (

Fig. S2 (A) illustrates the schematic diagram of impedance cytometry, which consists of a homemade measuring circuit and a FPGA-based LIA. First, the current signals from two output electrodes, triggered by flowing objects, are converted into voltage signals in Transimpedance Amplifier (TIA). The TIA was made with operational amplifier (OPA 657U), and the feedback resistor was selected as 33 k$\Omega$ for the best performance in this case. Then, the voltage signals from the TIA were sent into a differential amplifier (AD 8138) to calculate the differential voltage signals between two output electrodes. The fluctuation in differential voltage can be detected by the input side of the FPGA-based LIA through analog-to-digital converter (ADC) with a sampling frequency of 100 mega samples per second (MSPS), which is more than 10 times larger than the frequency of target voltage signal (6 MHz and 500 kHz).

In this work, we applied (Xilinx ZYNQ7020) (Fig. S2(B)) to prepare the LIA. Fig. S2B depicts the detection algorithms. The codes were compiled using VIVADO 2020.2. Inside the FPGA platform, a digital signal generator generates the reference signals (i.e., the in-phase and quadrature signals), one of which is given as the excitation voltage (2.6 V peak-to-peak) for the impedance cytometry. In the experiment, the frequency was set to 6 MHz and 500 kHz, and the frequency is equal to the frequency of the signal to be measured from the output sides. Then, the measured voltage signal was modulated with the in-phase and quadrature signals via digital multipliers in real time, resulting in two components (i.e., DC components and high-frequency components). After that, both results were sent to the next stage – the cascaded integrator–comb (CIC) filter cascade, in which the sampling frequency was reduced to 10 KSPS to eliminate most high-frequency components. To further reduce noise, we used a finite impulse response (FIR) filter with an order of 101 (Peled and Bede Liu, 1974). The filter design was achieved using MATLAB 2020a (Mathworks Inc., Natick, USA). The outputs from the FIR filter were converted to analog signals again (DIGILENT Pmod DA2, National Instruments), recorded by the data collection system (USB-6363 BNC, National Instruments, USA) and presented in computer. Since the response time of the detection system is set to 100 μs, the highest throughput of the detection system is limited to 125 ksamples/s.

# 3.    Simulation

To demonstrate impedance cytometry with different electrode layouts can be used as a shape sensor, we first performed 3D simulation of the impedance signals measured from "out" side of parallel electrodes for different shaped particles. Fig. S3 depicts the relationship between the shape of impedance pulses and the shape of the target particles when parallel electrodes are used. The microfluidic channel used in the simulation is 30 μm in depth and 40 μm in width, and patterned electrodes (30 μm in width) has a span of 30 μm. There are six types of particles with different shapes and sizes flowing through the detection area, and resultant impedance pulses have shown a clear shape dependence. For example, when the size of objects (Particle 1-3) is smaller than the electrode span, the peak of impedance pulses is at the center of span for spherical particle (Particle 1), but the pulses triggered by the conical particles (i.e., Particles 2-3) are asymmetric and the peak position depends on the orientation of the target particle. When the size of objects is larger than the electrode span, the shift of the impulse peak become clearer for particles with asymmetric morphology (i.e., Particle 5-6).
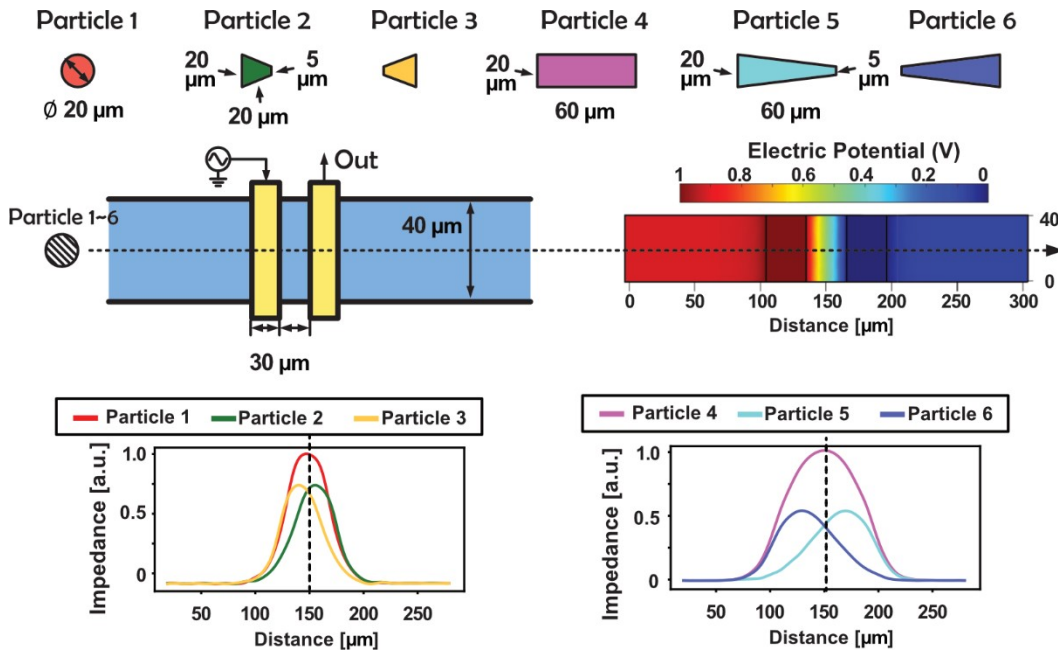
Fig. S3: Simulation for the dependency of the shape of impedance signals on the shape of target particles, when parallel electrodes are used.

We also performed simulation of impedance signals of nonparallel electrodes used in our previous study for particles of different shapes and different trajectories

(see Fig. S4). The impedance cytometry with nonparallel electrodes is sensitive to the size/shape of the target particles, and also has the capability to track the trajectory of particles in the microchannel. As shown in Fig. S4, the shape of objects (particle 1-2) can induce the tilting trend of the impedance pulses, and the trajectory of the particle can affect the impedance amplitudes.

In this work, we did not take the trajectory of *E. gracilis* cells into consideration, and our goal is to find the relationship between intracellular components and impedance signals. Therefore, we used the parallel electrodes instead of the nonparallel ones.
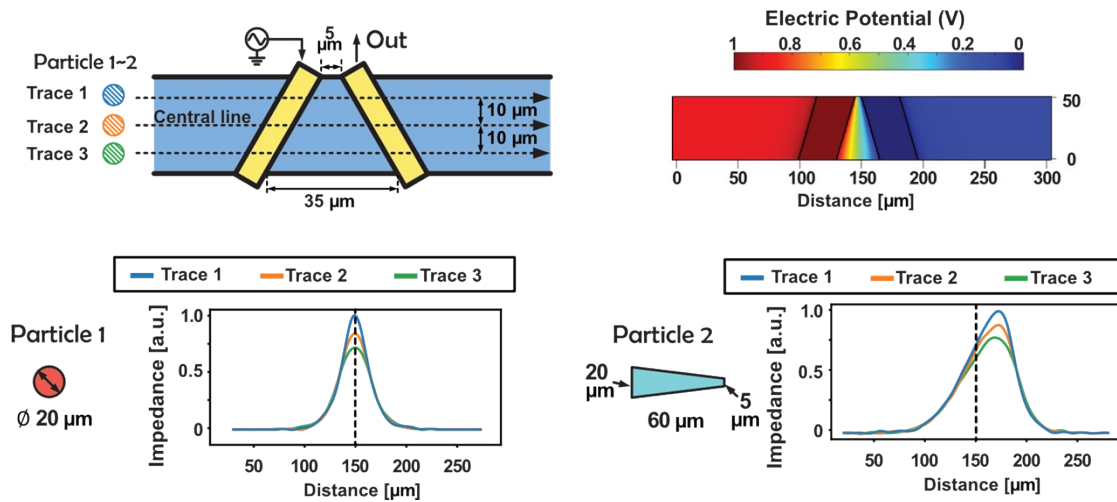


Fig. S4: Simulation for the dependency of the shape of impedance signals on the shape and trajectory of target particles, when nonparallel electrodes are used.

# 4.  Volume and occupancy

Table S1: Electrical diameter of samples

| Targets | Electric extracellular diameter | | | Electric intracellular diameter | | |
|---|---|---|---|---|---|---|
| | Mean | Range (10%-90%) | CV% | Mean | Range (25%-75%) | CV% |
| 15 μm beads | 15.000 | 13.394-17.792 | 10.719 | 15.000 | 13.468-17.471 | 10.043 |
| Original E. gracilis | 19.695 | 17.356-22.103 | 9.433 | 17.477 | 15.375-19.590 | 9.502 |
| Anaerobic | | | | | | |
| 12 h | 15.779 | 13.021-18.578 | 14.508 | 14.029 | 10.994-16.868 | 16.623 |
| 24 h | 13.343 | 9.892-16.547 | 19.123 | 12.055 | 9.260-14.684 | 17.801 |
| 48 h | 10.861 | 9.460-12.283 | 10.265 | 9.496 | 8.182-10.838 | 10.876 |
| 72 h | 9.708 | 8.175-11.342 | 12.564 | 8.550 | 7.243- 9.972 | 12.160 |
| Aerobic | | | | | | |
| 12 h | 15.510 | 13.330-17.890 | 12.815 | 13.760 | 11.626-16.113 | 13.723 |
| 24 h | 14.474 | 11.416-17.801 | 16.915 | 13.066 | 9.941-15.969 | 17.429 |
| 48 h | 11.492 | 8.916-14.334 | 17.901 | 10.430 | 8.278-12.772 | 16.557 |
| 72 h | 10.290 | 9.117-11.674 | 11.104 | 9.144 | 8.046-10.379 | 10.841 |

Table S2: Electrical occupancy (opacity) of samples

| Targets | Opacity | | |
|---|---|---|---|
| | Mean | Range (10%-90%) | CV% |
| 15 μm beads | 1.000 | 0.892-1.105 | 8.314 |
| Original E. gracilis | 0.700 | 0.643-0.756 | 6.783 |
| Anaerobic | | | |
| 12 h | 0.704 | 0.543- 0.818 | 16.265 |
| 24 h | 0.753 | 0.637- 0.924 | 16.172 |
| 48 h | 0.671 | 0.576- 0.759 | 11.866 |
| 72 h | 0.688 | 0.593- 0.780 | 11.473 |
| Aerobic | | | |
| 12 h | 0.702 | 0.611-0.810 | 13.949 |
| 24 h | 0.740 | 0.601-0.832 | 13.737 |
| 48 h | 0.761 | 0.647-0.892 | 15.351 |
| 72 h | 0.707 | 0.615-0.797 | 11.769 |

# 5. Shape and distribution

Table S3: Titling index of samples

| Targets | Titling index (LF) – Extracellular shape | | | Titling index (HF) – Intracellular distribution | | |
|---|---|---|---|---|---|---|
| | Mean | Range (10%-90%) | CV% | Mean | Range (25%-75%) | CV% |
| 15 μm beads | 0.011 | -0.030-0.060 | 371.50 | 0.009 | -0.054-0.075 | 604.90 |
| Original E. gracilis | 0.011 | -0.015-0.046 | 488.27 | 0.012 | -0.063-0.096 | 636.96 |
| Anaerobic | | | | | | |
| 12 h | 0.009 | -0.025-0.046 | 971.81 | 0.023 | -0.104-0.146 | 753.13 |
| 24 h | 0.014 | -0.029-0.061 | 541.56 | 0.019 | -0.093-0.124 | 988.20 |
| 48 h | 0.017 | -0.024-0.06 | 297.42 | 0.021 | -0.182-0.238 | 987.84 |
| 72 h | 0.051 | -0.028-0.130 | 221.24 | 0.051 | -0.028-0.130 | 221.24 |
| Aerobic | | | | | | |
| 12 h | 0.008 | -0.028- 0.047 | 1087.9 | 0.009 | -0.106- 0.124 | 1421.9 |
| 24 h | 0.022 | -0.015- 0.063 | 406.13 | 0.015 | -0.087- 0.125 | 933.18 |
| 48 h | 0.019 | -0.020- 0.061 | 277.78 | 0.0152 | -0.109- 0.140 | 935.81 |
| 72 h | 0.023 | -0.010-0.056 | 256.50 | 0.023 | -0.011- 0.057 | 256.50 |